INFLUENCE OF ROTATION ON THE FLOW OVER CYLINDER AT RE=5000

***D.E. Aljure*[1], *I. Rodríguez*[1], *O. Lehmkuhl*[1,2], *C.D. Pérez-Segarra*[1], *A. Oliva*[1]**

[1] ***Heat and Mass Transfer Technological Center (CTTC), Universitat Politècnica de Catalunya BarcelonaTech. ETSEIAT, carrer Colom 11, 08222 Terrassa, Barcelona, Spain.***
cttc@cttc.upc.edu
[2] ***TermoFluids, S.L. Av. Jaquard, 97 1-E, 08222, Terrassa, Barcelona, Spain.***
termofluids@termofluids.com
cttc@cttc.upc.edu

Abstract

The turbulent flow around a rotating cylinder submerged in a uniform flow is simulated using direct numerical simulations (DNS) using a Reynolds number based on cylinder diameter D and free stream velocity U_∞ of $Re = 5000$. The rotation relation is in the range $0 \leq \alpha \leq 5$.

Rotation brings upon a fundamental change of the pressure distribution, the stagnation point shifts downward with increasing α, falling outside the cylinder for rotation rates $\alpha > 4$. The Magnus effect is observed: as α increases a lift force appears and the drag force is modified, reducing for $\alpha < 3$ and increases slightly for $\alpha > 3$, additionally Prandtl's limit for the lift coefficient, 4π, was exceeded in the present work. Flow instabilities present for $\alpha = 0$ are reduced for $\alpha \leq 2$ and disappear for higher rotation ratios. For $\alpha = 3$, the recirculation bubble loses the two vortex configuration to have only one recirculating vortex in the near wake and for $\alpha \geq 4$ norecircualtion vortices are seen.

1 Introduction

The flow around a rotating cylinder at $Re = U_\infty D/\nu = 5000$ (U_∞ corresponds to the far field velocity and D is the cylinder diameter) and rotation relation ranging $0 \leq \alpha = U_\infty/U_T \leq 5$ (U_T is the tangential velocity on the cylinder surface) is simulated using direct numerical simulations (DNS). Viscous forces cause the flow attached to the cylinder to rotate about, strengthening the flow on one side of the cylinder and acting against it on the opposite side. According to the Bernoulli equation, this effect implies a rise in the pressure on one side of the cylinder and lowering it on the other creating a lift force, also referred to as the Magnus effect. This geometry has been studied previously, especially for the laminar regime using both experimental techniques and two dimensional (2D) simulations.

Prandtl (1925 and 1926) performed experiments using a cylinder with end plates placed between two walls and using a cylinder rotation ratio up to $\alpha = 4$. He observed wake deflection and the appearance of a lift force. Additionally, theoretical analysis performed set a limit for the lift force, $C_{Lmax} = 4\pi$, however his experimental results yielded a lower lift coefficient.

Thom (1931 and 1934) performed measurements on a cylinder rotating with a rotation ratio $\alpha = 2$ describing the velocity field and surface pressure present, deepening the understanding on the flow topology for higher α and the relation between the lift and drag coefficient with rotation ratio.

Glauer (1957) performed a theoretical analysis for the rotating cylinder at high α such that the flow separation is suppressed. A power series expansion was used to describe the boundary layer flow on the cylinder and expressions for circulation and torque on the cylinder were derived. Results showed a different trend than those presented by Prandtl where a limit on the lift force was theorized. In Glauert's investigation the circulation increased with α and did not reach a limit.

Ludwig (1964) performed experimental measurements on the rotating cylinder case for low rotation rates ($\alpha \leq 0.3$). From his experimental data a criterion for identifying the flow separation points was created, predicting a linear relation of this separation point on the downstream-moving wall with the rotation ratio α.

Constanceau and Ménard (1985) investigated this flow configuration for Reynolds number up to 1000 and velocity ratios $\alpha \leq 3.25$ concluding that as the velocity ratio α increases, meandering in the wake decreases and the Strouhal number increases and that these phenomena are strongly dependent on the Reynolds number.

Chou (2000) performed two dimensional simulations for $Re = 1000$ and $\alpha < 3$, and $Re = 10000$ and $\alpha \leq 2$. The author did a topological analysis to locate stagnation points, finding they were in good agreement with previous references. Additionally, vorticity contours showed the formation of a Kármán vortex street for $\alpha = 1$. For $\alpha = 2$ the formation of the vortex street is delayed and for $\alpha = 3$ it is suppressed. Their results were in good agreement with experimental results for the initial transient period, however, a discrepancy is seen after the flow becomes turbulent (thus three di-

mensional).

Mittal and Kumar (2003) investigated via two-dimensional computations this case, with Reynolds $Re = 200$ and $Re = 1000$, and $0 \leq \alpha \leq 5$. Good agreement between results and previous studies was found. Results also showed that very large lift coefficients were observed for high rotation rates. The two-dimensional computations performed yielded higher lift coefficients than the theoretical limit. Similarly as before, von Kármán vortex street was seen for $\alpha < 1.9$. A second instability zone was identified for $4.35 < \alpha < 4.7$ where vortices are shed only from one side of the cylinder.

Lam (2009) investigated experimentally the flow past a rotating cylinder al $Re = 3600$-$Re = 5000$ at low rotation ratios ($\alpha < 2.6$). In agreement with the state-of-the-art vortex shedding was found to occur for rotation ratios lower than $\alpha = 1.9$ and that the vortex shedding frequency increases as the the rotation ratio increases. However, the value of vortex shedding reported at $\alpha = 0$ was of $St = 0.18$, which is lower than that reported in the literature ($St \approx 0.21$ Norberg (1994), amongst others). It is worth noting that the cylinder aspect ratio of the experiment was 11.6. Norberg (1994) showed that the flow exhibits large instabilities in the range of $Re = 1000$-$Re = 10000$ when it comes to the dependence with the cylinder aspect ratio and the size of the cylinder end plates. He found that variations in the vortex shedding frequency and base pressure become independent of the aspect ratio and end plates size for aspect ratios of about 70. This might explain why the vortex shedding frequency measured by Lam (2009) at $Re = 5000$, for the still cylinder, is considerably lower than the values reported in the literature.

The present work aims at shedding some light on the effect of the rotation ratio in the vortex shedding, drag and lift coefficients in transition turbulent flows using DNS in order to fully understand the physics involved and the influence of rotation in the flow topology. These issues are of major importance in many practical application e.g. marine structures, civil engineering, aerodynamic design, etc. Finally, it is also important to consider the reduction of flow induced vibrations and the role of the vortex shedding in this phenomenon. Simulations are performed using different meshes to correctly capture the three-dimensional structures present in the wake of the cylinder and the effects brought on by rotation.

2 Mathematical formulation

In order to solve the flow, the three dimensional - time dependent Navier-Stokes equations are solved:

$$\frac{\partial \mathbf{u}}{\partial t} + (\mathbf{u} \cdot \nabla)\mathbf{u} - \nu \nabla^2 \mathbf{u} + \rho^{-1} \nabla p = 0 \qquad (1)$$

$$\nabla \cdot \mathbf{u} = 0 \qquad (2)$$

where $\mathbf{u}$ is the three-dimensional velocity vector, p is the pressure scalar field, ν stands for kinematic viscosity and ρ for the density of the fluid.

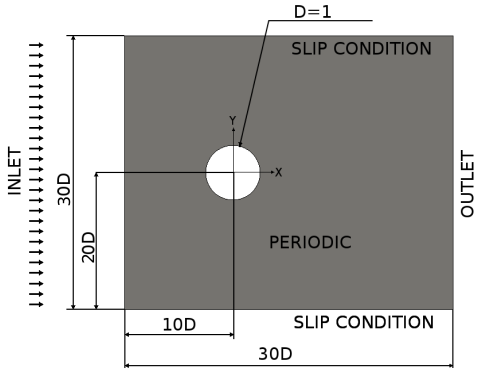

Figure 1: Computational domain.

The geometry to be considered is a cylinder with diameter D shown in figure 1 submerged in a uniform fluid flow and rotating with velocity ratio α in the clockwise direction. Simulations are carried out at a Reynolds number $Re = 5000$ based on the cylinder diameter and free stream velocity. The computational domain is $30D \times 30D \times 2\pi D$ in the stream-, cross-stream and span-wise directions. The center of the cylinder is located at a distance of $10D$ downwind from the inlet boundary and at a distance of $20D$ from the bottom boundary as shown in figure 1.

Governing equations (1 and 2) are discretized on a collocated unstructured mesh by means of finite volume techniques. A second-order conservative scheme is used for the spatial discretization (Verstappen and Veldman 2003). Such schemes preserve the symmetry properties of the continuous differential operators and ensure both stability and conservation of the kinetic-energy balance. The velocity-pressure coupling is solved by means of a fractional-step algorithm. The temporal discretization for the convective, diffusive and derivative terms was made using a second order self-adaptive scheme (Trias and Lehmkuhl 2011); whereas a backward Euler scheme was used for the pressure gradient. For more details about the discretization the reader is referred to Jofre et al. 2014 and Trias et al. 2014. Meshes are constructing by using a constant-step extrusion of a 2D mesh. Under these conditions, the Poisson equation can be solved by means of a Fast Fourier Transform (FFT) method. This diagonalization decouples the 3D system into a set of uncoupled 2D subsystems which can be solved by means of a Direct Schur-complement decomposition method (Borrell et al. 2011). Present numerical model and discretization technique has been successfully used in solving transition Reynolds number flow over cylinders (Lehmkuhl et al. 2013) and a sphere

(Rodríguez et. al 2011).

Table 1: Mesh parameters. CV_{plane} is the number of control volumes in the plane, N_{planes} is the number of planes in the span-wise direction, NCV the total number of control volumes in the domain.

α	CV_{plane}	N_{planes}	NCV
0	88519	256	2.26×10^7
	115709	320	3.70×10^7
1	95030	256	2.43×10^7
	123145	320	3.94×10^7
2	97887	256	2.5×10^7
	130020	320	4.16×10^7
3	127234	320	4.07×10^7
	133145	320	4.26×10^7
4	127234	320	4.07×10^7
	138461	320	4.43×10^7
5	127234	320	4.07×10^7
	147591	320	4.72×10^7

Table 1 shows information on the meshes used for the present study. Two meshes were used for each rotation ratio. Meshes for the lower α's use two different span wise resolution whereas the meshes used for higher α, due to the increased difficulty in the boundary layer resolution use the higher span wise resolution for both meshes.

Table 2: Non-dimensional wall distance (y^+) values

α	0	1	2	3	4	5
y^+1_{MIN}	0.12	0.05	0.04	0.05	0.04	0.05
y^+1_{MAX}	2.72	3.01	2.23	2.63	2.80	3.08
y^+1_{MEAN}	0.95	1.50	1.28	1.41	1.47	1.85
y^+2_{MIN}	0.14	0.06	0.2	0.16	0.06	0.1
y^+2_{MAX}	3.46	3.57	3.07	3.68	3.85	4.15
y^+2_{MEAN}	1.29	1.79	1.86	1.95	1.96	2.22

Mesh refinement is done in the near-wall area to improve resolution of the boundary layer. Table 2 shows values for the distance to the wall in wall units for the first two nodes in the finer meshes. The location of the two first nodes is of great importance for the correct resolution of the boundary layer flow. Within the viscous sublayer, defined for $y^+ \lesssim 5$, viscous stresses are the dominating force in the flow. Meshes used in the present investigation have, at least, the first two nodes in the boundary layer fall within the viscous sub-layer to ensure its correct resolution.

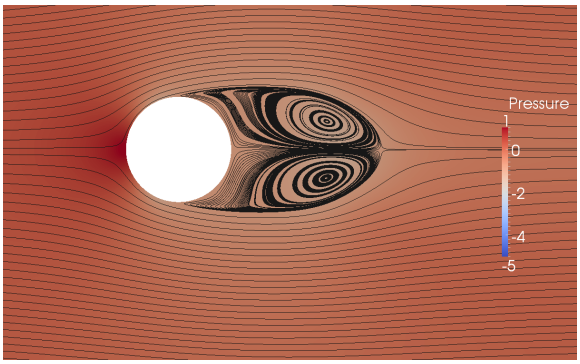

(a) $\alpha = 0$

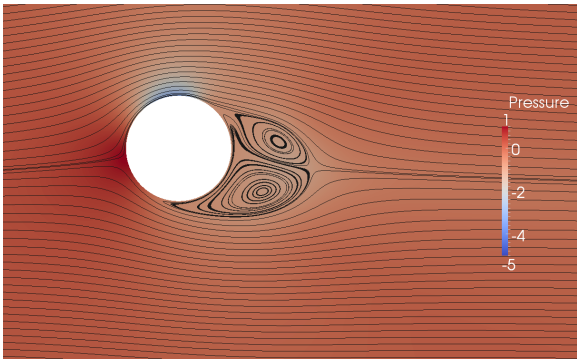

(b) $\alpha = 1$

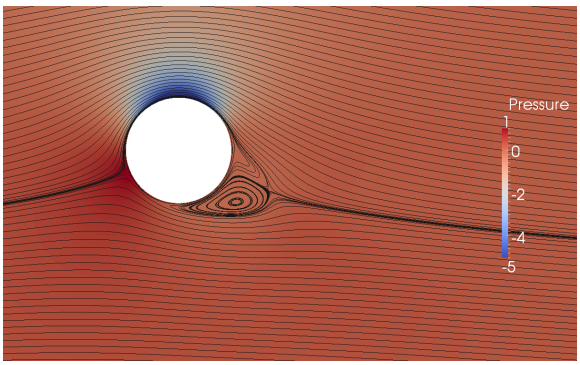

(c) $\alpha = 2$

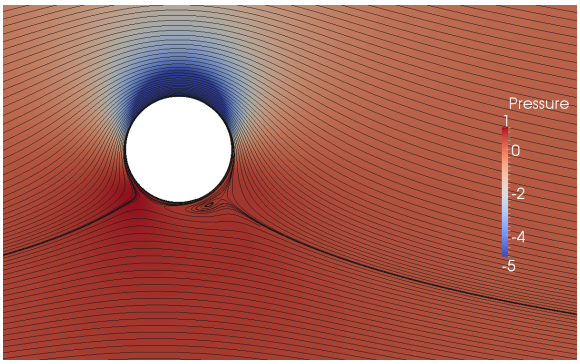

(d) $\alpha = 3$

Figure 2: Averaged streamlines, colored by pressure.

3 Results

Figure 2 shows the averaged in time and span wise direction streamlines in the x-y plane. For $\alpha = 0$ and $\alpha = 1$ a two vortex configuration is seen, being the top vortex smaller for $\alpha = 1$. For $\alpha = 2$ the top vortex is almost gone and bottom vortex has reduced its size considerably, whereas for $\alpha = 3$ top vortex is has dissapeared and the bottom one is barely visible.

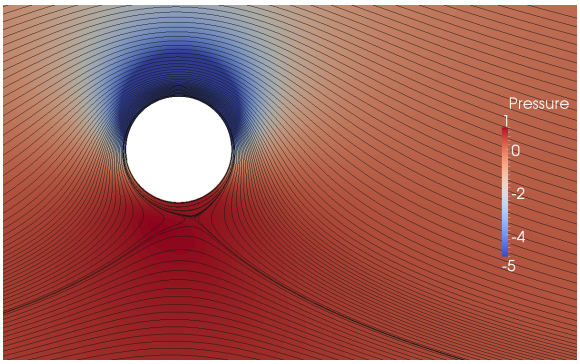

(e) $\alpha = 4$

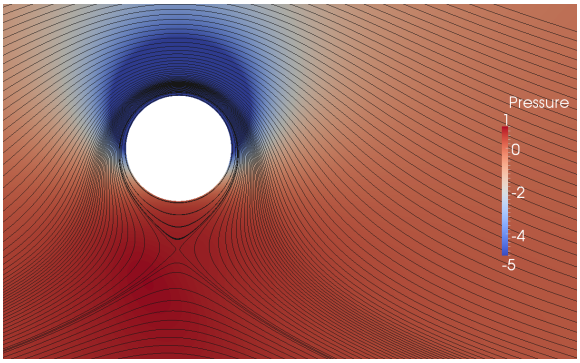

(f) $\alpha = 5$

Figure 2: Cont. Averaged streamlines, colored by pressure.

Rotation relations between $\alpha = 0$ and $\alpha = 3$ all have the stagnation point within the cylinder surface and the saddle point in the edge of the recirculation region. A different flow configuration is observed for $\alpha = 4$ and $\alpha = 5$. For the higher rotation ratios no vortices in the recirculation area are clearly visible. Additionally, the stagnation point is now located off the cylinder and coincides in location with a saddle point.

Figure 3 shows the mean pressure distribution around the cylinder surface, where 0° corresponds to the front of the cylinder. Angles are measured in a counter clock wise direction. There are three aspects to observe in this figure: stagnation point, base pressure and pressure minimum. Cylinder rotation induces a shift in the stagnation point. Locations for this parameter can be seen in table 3. Oncoming flow attaches to the front of the cylinder as it rotates. For $\alpha = 0$ the stagnation point is placed on the symmetry plane, however, as α increases an upward motion is gained by the fluid in front of the cylinder. This upward motion bends the incoming flow, shifting the stagnation point's location.

For $\alpha = 0$ base pressure is constant and behind the cylinder. As α increases its location shifts downward dragged by the rotation motion and it spans for a smaller arch due to the influence of the low pressure zone from the top. Rotation effect on this parameter can be divided in three segments: $\alpha = 0$ and $\alpha = 1$, where base pressure remains nearly constant,

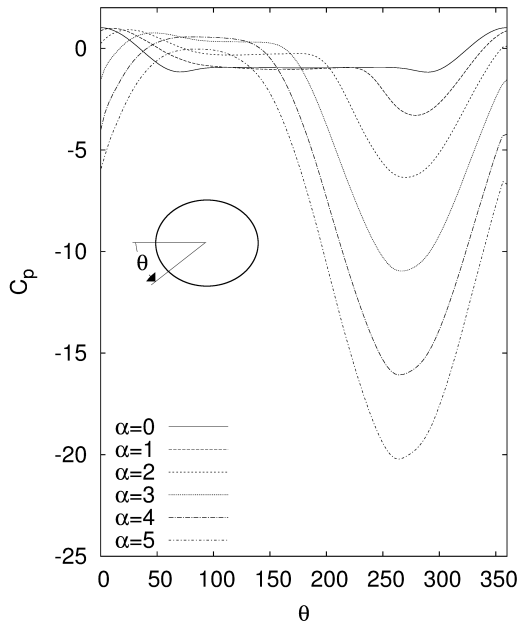

Figure 3: Local pressure coefficient at different rotation ratios.

Table 3: Pressure parameters

α	Stag. Point	Base Press.	Press. Min.
0	0°	-0.94	-1.2
1	10°	-0.99	-3.3
2	30°	-0.32	-6.4
3	45°	0.32	-10.9
4	101.5°*	0.54**	-16.2
5	89.4°*	0.05**	-20.6

* Stag. point off the cylinder
** Pressure maximum in the cylinder surface

influenced by the flow separation that creates the large recirculation region seen in figure 2. As α increases to $\alpha = 2$ and $\alpha = 3$ there is a rise in the base pressure reducing the size of the recirculation vortices. This effect is brough upon by the attachment of the boundary layer to the cylinder and the delay in its separation. Finally, for $\alpha = 4$ and $\alpha = 5$ a recirculating layer forms around the cylinder eliminating the base pressure and, thus, the recirculation region.

The pressure coefficient minimum on the cylinder surface is also quite affected by the cylinder rotation. As stated earlier, the flow attached to the cylinder rotates about with it. Fluid velocity on top of the cylinder increases as the rotation ratio α does, inducing, by means of the Bernoulli effect, a drop in pressure. Values for this parameter are presented in table 3.

Table 4 shows the drag and lift forces relation with rotation relation α. As the rotation parameter increases there is a significant increase in the lift force. Prandtl (1925) stated that the maximum lift in such configu-

Table 4: Force coefficients

α	0	1	2	3	4	5
Drag	1.05	0.90	0.36	0.18	0.25	0.64
Lift	0.00	1.40	4.47	8.93	13.21	16.01
C_L/C_D	0.00	1.56	12.42	49.61	52.84	25.02

ration is limited to 4π, however, different authors report quite different solutions (Mittal and Kumar 2003). Present results, although larger than the theoretical limit proposed by Prandtl (1925), are lower than those presented by other authors that performed 2D simulations (Stansby and Rainey 2001, Mittal and Kumar 2003). The behavior of the drag coefficient follows a different trend than the lift coefficient. After reducing between $\alpha = 0$ and $\alpha = 3$, there is a slight increase in this parameter for $\alpha = 4$ and $\alpha = 5$, due to the shift of stagnation point off of the cylinder, the base pressure span and location changes, and suppression of the recirculation vortices. Finally, the ratio C_l/C_D follows two different trends, for $\alpha \leq 3$ it follows an increasing-exponential trend. For $\alpha \geq 4$ the trend is decreasing.

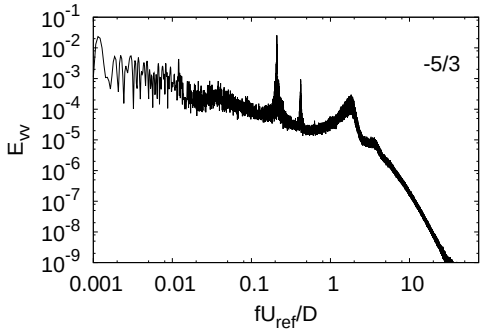

(a) $\alpha = 0$

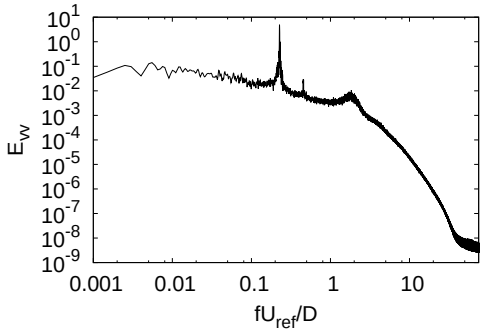

(b) $\alpha = 1$

Figure 4: Power Spectra

Figure 4 shows the power spectra for a point within the shear layer in each rotation ratio. For $\alpha = 0$ and $\alpha = 1$ energy peaks can be observed for the vortex shedding frequency (primary frequency) and for the

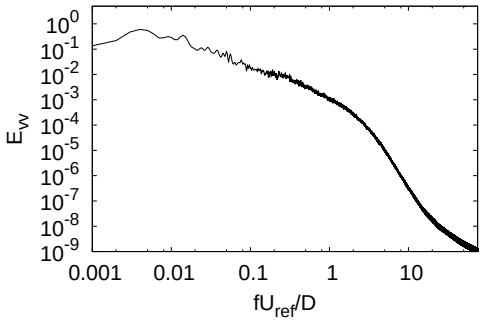

(c) $\alpha = 2$

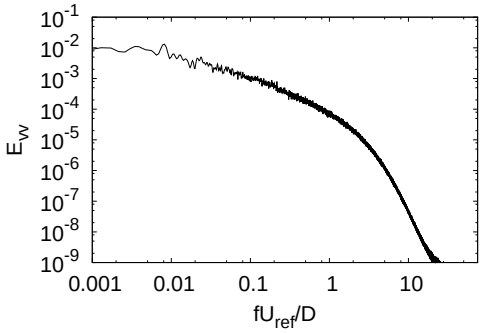

(d) $\alpha = 3$

Figure 4: Cont. Power Spectra

Table 5: Dominating frequencies (St)

α	0	1	2	3	4	5
Primary	0.209	0.223	-	-	-	0.046
Secondary	1.83	1.80	-	-	-	0.067

shear layer frequency (secondary), see table 5. It is important to note that as rotation ratio increases from $\alpha = 0$ to $\alpha = 1$ both the vortex shedding and Kelvin-Helmholtz energy peaks decrease in magnitude and gain bandwidth, indicating that the periodic behavior that characterizes the vortex shedding phenomenon is growing weaker. For $\alpha = 2$, $\alpha = 3$ and $\alpha = 4$ no such peaks can be seen. For $\alpha = 5$ a twin peak energy surge is observed, indicating some kind of periodic behavior. Similar peaks were also observed at this rotation ratio for lower Reynolds numbers (Stojkovic et al. 2002).

In this work coherent structures are analyzed by means of the Q-criterion which identifies a vortex in a region where the second invariant of the velocity gradient tensor is positive ($Q > 0$), being $Q = 0.5(||\Omega^2|| - ||S^2||)$, with $||\Omega||$ and $||S||$ the trace of the skew-symmetric and symmetric components of $\nabla \mathbf{u}$. Positive values of Q correspond to an area where rotation is greater than strain (Hunt et. al. 1988).

Figure 5 shows the side view of the $Q = 3$ surfaces showing the fundamental change brought upon by the rotation of the cylinder. Flow topology does

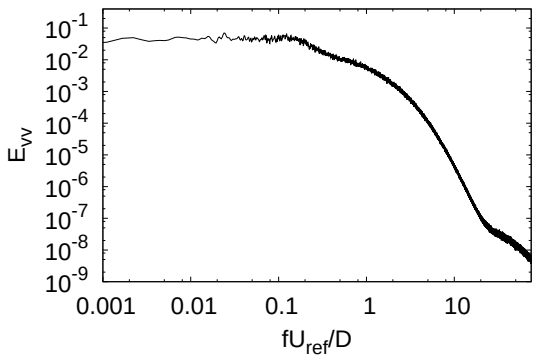

(e) $\alpha = 4$

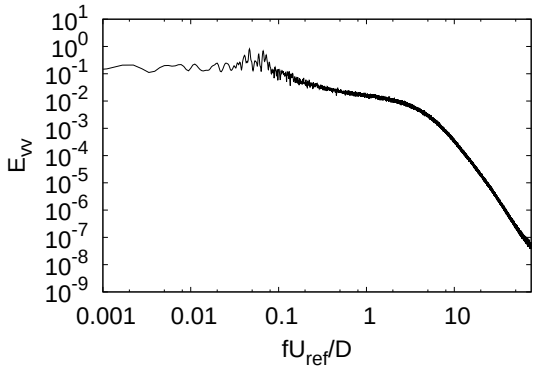

(f) $\alpha = 5$

Figure 4: Cont. Power Spectra

(a) $\alpha = 0$

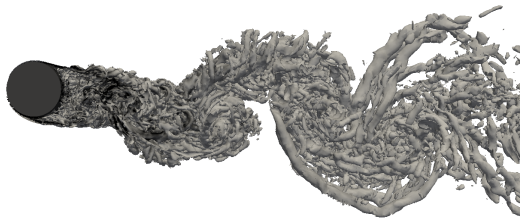

(b) $\alpha = 1$

Figure 5: $Q = 3$ isosurfaces.

not change dramatically between $\alpha = 0$ and $\alpha = 1$ where the von Kármán vortex street and shear layers are visible. Additionally, the wake is composed of larger structures than for greater rotation relations.

For $\alpha = 2$ the top shear layer ceases to interact with the bottom one, causing vortex shedding to cease and the wake is influenced mainly by the flow coming from the bottom of the cylinder. The vortex street

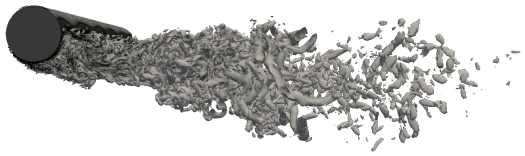

(c) $\alpha = 2$

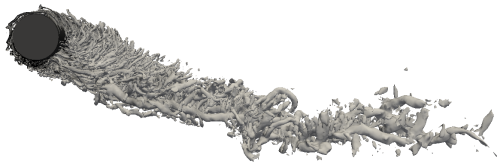

(d) $\alpha = 3$

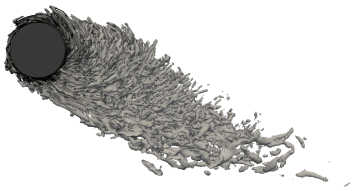

(e) $\alpha = 4$

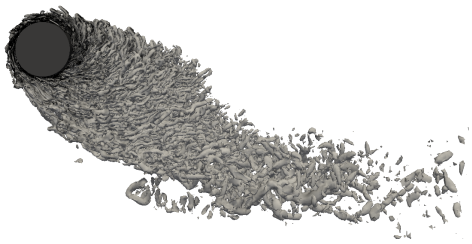

(f) $\alpha = 5$

Figure 5: Cont. $Q = 3$ isosurfaces.

structure has been damped down by the decreasing influence of the shear layers in the wake flow, reaching the point where it no longer seems to be influenced by the flow coming from the top of the cylinder. The wake is now composed of small, independent vortices that detach in an un-organized fashion from the geometry.

For $\alpha = 3$ shear layers are no longer visible, in place is now a recirculating layer around the surface. This structure now influences the wake formation and its flow configuration. The disappearance of the top recirculation vortex in the wake plays a fundamental role in the changes seen in wake topology. As α increases from $\alpha = 0$ to $\alpha = 3$ this structure shrinks, from a symmetrical two vortex configuration in $\alpha = 0$ to a asymmetrical single vortex configuration in $\alpha = 3$ where the top vortex has disappeared and the bottom vortex is very small in comparison to those present in smaller α. For $\alpha = 3$ and $\alpha = 4$ the wake is thinner than for the other rotation ratios, coinciding with where the drag coefficient is at its lowest.

For $\alpha = 4$ the stronger, recirculating layer around the cylinder and the dissapperance of the recirculation vortices further shrinks the wake structures and causes

the near wake to grow in the crossflow direction. Furthermore, this effect is amplified when the rotation ratio increases to $\alpha = 5$.

4 Conclusions

- The primary effect of rotation is seen on the shear layer. Rotation bends this structure behind the cylinder until, for higher rotation ratios, it turns into a recirculating layer. When this structure is affected consequences are seen through out the wake, leading to the conclusion that this is the most important structure in this flow geometry. Top shear layer is most affected by rotation, causing the symmetry to be broken. Additionally, flow structures, wake topology and force coefficients show a different trend for $\alpha \leq 3$ than for $\alpha \geq 4$.

- Vortex shedding was observed for rotation rates $\alpha = 0$ and $\alpha = 1$, additionally, for low rotation rates flow dynamics do not vary much. Key characteristics, e.g. shear layers and vortex shedding, are still present. Shear layer instability is reduced, which in turn reduce the overall instability in the flow; the top shear layer still exists and is able to interact with its counter part from the bottom, and thus, maintaining the vortex shedding. This phenomenon disappears for larger α; a value of $\alpha \approx 1.9$ is documented as the limiting rotation ratio for vortex shedding. For $\alpha > 2$ flow dynamics change substantially, as the flow characteristics mentioned before change.

- The pressure distribution shifts due to the rotation of the cylinder. The pressure drop on top increases non-linearly with rotation ratio α, keeping the absolute minimum in pressure in this part. As the top shear layer is weakened it no longer interacts with the bottom shear layer causing the base pressure to rise as well, however, between $\alpha = 3$ and $\alpha = 4$ this parameter stops its increasing trend and decreases for $\alpha = 5$.

- Prandtl's limit for lift coefficient, 4π, was exceeded in the present work, however, lift results from the present investigation are lower than 2D results published by different authors and lower than the lift coefficient predicted by the potential flow theory ($2\pi\alpha$). Drag coefficient, after reducing between $\alpha = 0$ and $\alpha = 3$ increases for $\alpha = 4$ and $\alpha = 5$ due to the change in flow configuration, the shift in the stagnation point and pressure coefficient distribution in the cylinder surface.

Acknowledgments

This work has been partially financially supported by the "Ministerio de Economía y Competitividad, Secretaría de Estado de Investigación, Desarrollo e Innovación", Spain (project ref: ENE2010-17801), by the colaboration project between "Universitat Politècnica de Catalunya" and Termo Fluids S.L. and by the "Departamento Administrativo de Ciencia, Tecnología e Innovación - Colciencias" via their doctoral training program "Francisco Jose de Caldas". We also acknowledge the access to MareNostrum Super-Computer III granted by the "Red Española de Supercomputación"

References

Borrell R, Lehmkuhl O, Trias F, Oliva A. (2011), Parallel direct Poisson solver for discretisations with one Fourier diagonalisable direction.*Comput. Phys.* Vol 230(12), pp 472341.

Chou, M.-H. (2000). Numerical study of vortex shedding from a rotating cylinder immersed in a uniform flow field. it Int. J. Numer. Meth. Fluids 32, pp 545-567.

Coutanceau, M., Ménard, C. (1985), Influence of rotation on the near-wake development behind an impulsively started circular cylinder. *J. Fluid Mech.* Vol 158, pp 399-446.

Glauert, M. B. (1957). The flow past a rapidly rotating circular cylinder. *Proceedings of the Royal Society of London. Series A, Mathematical and Physical Sciences* 242.

Hunt, J. C. R., Wray, A. A., and Moin, P., (1988). Eddies, stream and convergence zones in turbulent flows. *In: Proceedings of the Summer Program*.

Jofre, L., Lehmkuhl, O., Ventosa, J., Trias, F. X., and Oliva, A. (2014),Conservation properties of unstructured finite-volume mesh schemes for the Navier-Stokes equations. *Numer. Heat Tr. B-Fund.* Vol 64 (1), pp 53-79.

Ludwig, G. R. (1964). An experimental investigation of laminar separation from a moving wall. *AIAA- Aerospace science meetings* (64-6).

Lam K.M. (2009), Vortex shedding flow behind a slowly rotating circular cylinder. *J. of. Fluid and Structures* Vol 25, pp 245-262.

Lehmkuhl, O., Rodríguez, I., Borrell, R., Pérez-Segarra, C. D., Oliva, A. (2013), Low-frequency variations in the wake of a circular cylinder at Re=3900. *Phys. of fluids* vol 25 (8), 085109.

Mittal, S., Kumar, B. (2003), Flow past a rotating cylinder. *J. Fluid. Mech.* Vol 476 pp 303-334.

Mittal, S. (2004), Three-Dimensional Instabilities in flos past a rotating cylinder. *J. of applied Mech.* Vol 71, pp 89-95.

Norberg, C., (1994). An experimental investigation of the flow around a circular cylinder: influence of aspect ratio. *J. of Fluid. Mech.* Vol. 258.

Prandtl, L. (1925). The Magnus effect and windpowered ships. *Die Naturwissenchadten* 6, 94-108.

Prandtl, L. (1926). Application of the Magnus effect to the wind propulsion of ships. *Technicalmemorandums, National advisory comittee for aeronautics* 367.

Rao, A. Leontini, J. Thompson, M. C. and Hourigana K. (2013), Three-dimensionality in the wake of a rotating cylinder in a uniform flow. *J. Fluid Mech.*Vol 717, pp 1-29.

Rodríguez, I., Borrell, R., Lehmkuhl, O., Pérez-Segarra, C. D., Oliva, A., (2011), Direct numerical simulation of the flow over a sphere at Re=3700. *J. o f Fluid Mech*. Vol

25 (25), 263-283.
Stansby, P. K., Rainey, R. C. T. (2001), A CFD study of the dynamic response of a rotating cylinder in a current. *J. Fluids Struct.* Vol 15, pp 513-521.
Stojkovic, D., Breuer, M. and Durst, F. (2002), Effect of high rotation rates on the laminar flow around a circular cylinder. *Phys. of fluids* Vol 14, (9).
Thom, A. (1931). Experiments on the flow past a rotating cylinder. *Aeronautical research commitee, Reports and memoranda* 3095.
Thom, A. (1934). Effect of discs on the air forces on a rotating cylinder. *Aeronautical researchcommitee, Reports and memoranda* 3488.
Trias, F. and Lehmkuhl, O. (2011), A Self-Adaptive Strategy for the Time Integration of Navier-Stokes Equations. *Num. heat transfer, Part B, fundamentals.* Vol 60, pp 116-134.
Trias, F. X., Lehmkuhl O., Oliva, A., Pérez-Segarra, C. D. and Verstappen, R.W.C.P. (2014), Symmetry-preserving discretization of NavierStokes equations on collocated unstructured grids. *J. of Comp. Phys.*, Vol 258, pp 246-267.
Verstappen, R. W. C. P. and Veldman, A. E. P. (2003), Symmetry-preserving Discretization of Turbulent Flow. *J. Comp. Phys.* Vol 187, pp 343-368.